ISSN 0742-0463, Journal of Volcanology and Seismology, 2020, Vol. 14, No. 4, pp. 246–261. © Pleiades Publishing, Ltd., 2020.
Russian Text © The Author(s), 2020, published in Vulkanologiya i Seismologiya, 2020, No. 4, pp. 40–56.

The Mineralogical and Geochemical Properties of Near-Crater Tephra from Erebus Volcano, Antarctica Based on the Ejecta of the 2000 Eruption

V. I. Silaev[a], *, G. A. Karpov[b], **, V. N. Filippov[a], B. A. Makeev[a], S. N. Shanina[a], A. F. Khazov[a], and K. V. Tarasov[b]

[a] *Institute of Geology, Komi Science Center, Ural Branch, Russian Academy of Sciences, ul. Pervomaiskaya, 54, Syktyvkar, 167982 Russia*

[b] *Institute of Volcanology and Seismology, Far East Branch, Russian Academy of Sciences, bulvar Piipa, 9, Petropavlovsk-Kamchatsky, 683006 Russia*

**e-mail: silaev@geo.komisc.ru*

***e-mail: karpovga@ksnet.ru*

Received November 12, 2019; revised February 5, 2020; accepted March 31, 2020

Abstract—Multidisciplinary petrologic, mineralogical, and geochemical studies have been carried out for the first time concerning near-crater tephra from the world-largest intraplate stratovolcano (Erebus). The volcano is characterized by a unique basanite–phonolite effusive lineage. We studied the grain-size and chemical compositions of the tephra and the concentration of trace elements in it, the mineral phase composition, lithogenic gases encapsulated in the tephra, an atomically dispersed carbonaceous substance, and the isotope composition of carbon in it. We came to the conclusion that the tephra studied here can be treated as an explosive analogue of anorthoclase lava phonolites that terminate the continuous series of magmatic differentiates known as the Erebus lineage.

Keywords: Erebus, Erebus magmatic lineage, tephra, anorthoclase, fluochlorohydroxylapatite, monazite, barite, magnetite, native metals, chloride solid solutions

DOI: 10.1134/S0742046320040053

INTRODUCTION

Erebus (Fig. 1) is an active intraplate stratovolcano (standing on the volcanic Ross Island, 77°32′ S, 167°17′ E) on a thin (17–25 km) continental crust. It is confined to the edge of the West Antarctic Rift System (Kyle et al., 1992; *Encyclopedia ...,* 1999). The volcano is 1.3 Ma old, with its recorded activity being known for the past 172 000 years (Late Pleistocene to the present). That period saw numerous, mostly effusive, eruptions, with the activity peaking in the time spans 95 ± 9... 76 ± 4 and 27 ± 3 ... 21 ± 4 ka (Harpel et al., 2004; Esser et al., 2004; Kelly et al., 2008]. The associated lavas have a composition to make a nearly continuous sequence of magmatic differentiation (the so-called Erebus lineage) in the following sequence: basanites (olivine tephrite) → phonotephrite → tephrophonolite → anorthoclase phonolite (Iacovino et al., 2013; Iverson et al., 2014). The phonolite fraction in the sequence is 20–30%. The rock forming minerals of the lavas were found to be olivine ranging between $Fa_{55–88}$ in basanite and $Fa_{43–51}$ in the phonotephrite; aegirine-augite; Mn–Mg–Al–Cr-bearing ulvite-magnetite; hexagonal pyrrhotine of the $Fe_{0.96–1}S$ composition concentrating in interstitial magnetite; feldspar ranging from orthoclase-albite-anorthite in basanites to anorthite-orthoclase-albite in phonolites; nepheline, whose concentration increases in the direction from basanite to phonotephrite. The magnetite–ilmenite thermometer gave a temperature of 1081 ± 12°C for crystallizing basanite lava (Kyle et al., 1992).

Mount Erebus has demonstrated a stable phonolite composition of its eruptions during the past 40000 years, i.e., for nearly all Quaternary time. The volcano has been in an active phase since the 1970s; it has a persistent lava lake in the crater, and periodically discharges pyroclastic material (Taziev, 1987).

In addition, lava trachytes were detected on Erebus; these are considered to be a special incidental magmatic derivate resulting from a combined fractional assimilation crystallization.

Examination of petrologic and geochemical data suggested that the primary basanite melt occurs at Erebus by 2% melting of peridotite in a pulsating high (plume) of a depleted asthenosphere mantle directly beneath the volcano. The plume diameter is approximately estimated as 40 km(Kyle et al., 1992). The iso-

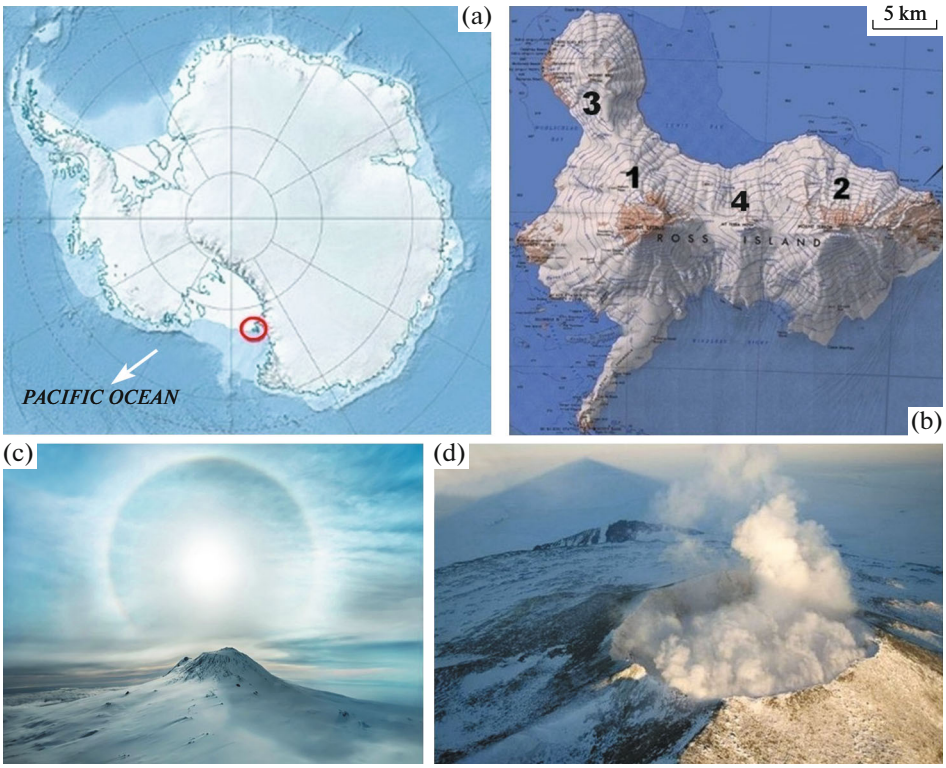

Fig. 1. Antarctica (a); volcanic Ross Island (b) with volcanoes: Erebus ((*1*) height 3794 m, crater 805 m across and 274 m deep), Terror ((*2*) 3230 m), Bird ((*3*) 1765 m), Terra Nova ((*4*) 2130 m); Mount Erebus (c) and Erebus crater (d) at dawn.

tope ratios $^{87}Sr/^{86}Sr = 0.702984 \pm 0.000028$ and $^{143}Nd/^{144}Nd = 0.5102 \pm 0.0019$ obtained for the Erebus effusive rocks are characteristic of the West Antarctica Cenozoic rift volcanoes (Panter et al., 2006) for OIB basalts in general. Each generation of basanites at Erebus is supposed to come from a new portion of mantle melt, with the subsequent fractional differentiation of the basanite melt occurring at high temperatures and under relatively dry conditions (Iverson et al., 2014).

There is a higher $^{87}Sr/^{86}Sr$ ratio (0.70425), for lava trachytes, which supports the hypothesis that they were formed by combined fractional assimilation crystallization.

Explosive events in the history of Erebus were recorded much rarer, with the most reliable dates being in the time spans 77–56, 46–32, and 18–10 ka. Traces of eruptions were detected in ice cores, providing evidence of as many as 14 dated and 20 undated (so far) tephra layers. All of this shows that explosive activity has been far less frequent than effusive activity at Erebus, and occurred as discrete events, but still is present throughout the entire eruption record (Harpel et al., 2004). The most recent period of effusive and explosive activity at Erebus began in 1972, inaugurating the modern epoch of systematic studies in the ejecta of Cenozoic volcanism in Antarctica (Kyle and Jazek, 1978; Stothers and Rampino, 1983).

THE OBJECT OF STUDY AND THE METHODS USED

The object was a small amount of comparatively fresh, light-colored ash that was thought to come from the 2000 eruption that Ph.R. Kyle sampled at the rim of the Erebus crater. The particles in the sample mostly have elongate shapes, varying between 200 and 1000 μm across (Fig. 2). The sample was studied using the following techniques: optical microscopy (an OLYMPUS BX51 computerized unit); X-ray diffractometry (Shimadzu XRD-6000); analytic scanning electron microscopy (JSM-6400 with EDX and wave spectrometers); inductively coupled plasma mass spectrometry (Perkin Elmer ELAN 9000); X-ray fluorescence spectrometry (Shimadzu XRF-1800); isotope spectrometry (Delta V+ (Finnigan) with a Flash EA-HT 1112 elemental analyzer and a ConFlo IV gas commutator); gas chromatography (Tsvet-800 with a pyrolysis device). Analysis for trace elements was performed at the *Geoanalitik* TsKP, Institute of Geology and Geochemistry, Ural Branch (UrB), Russian Academy of Sciences (RAS) (Yekaterinburg), the other determinations were carried out at the *Geonauka* TsKP, Institute of Geology, Federal Research Institute, Komi Science Center, UrB RAS (Syktyvkar).

Fig. 2. The morphology and sizes of tephra particles in the sample taken from Mount Erebus.

PARTICLE HABITUS AND SIZE

With respect to morphology and size, the particles in the sample subdivide into four types (Table 1). The *first* type includes the largest, elongate, nearly prismatic forms (with an elongation index of 2.5–3) that consist of intergrowths of numerous fiber-like subindividuals 10–30 μm thick (Figs. 3a–3f). The end parts of these particles contain rather deep cavities that have their axes nearly parallel to the length of the subindividuals and are very similar to gas bubbles emerging during degassing of a cooling melt (see Figs. 3e, 3f). The cavities are oriented along the direction of fiber subindividuals in the particles, which is quite consistent with the idea of their origin. The *second* type includes somewhat smaller and less elongate (the elongation index 1.3–1.7) angular lumpy particles having smooth-walled, isometric and oval cavities; these are even more similar to bubbles that have lost their gases as time went on.

The *third* type includes numerous horned particles (Figs. 4a–4f) that have sizes and elongations similar to the angular lumpy particles. They too typically contain bubbles, but their sizes vary in a larger range, from relatively large ones of 20–30 μm to smaller, 1–5 μm, which are also oval or round. Lastly, we classified the *fourth* type as including almost the most frequent tabular forms with small-step lateral planes (see Figs. 4g–4l). Bubbles are extremely rare on these particles.

Table 1. The morphologic types and sizes of particles in the tephra sample studied

Particle type	Particles	Length, μm	Width, μm	Elongation index
I	Subprismatic	1396 ± 612 (44%)	475 ± 227 (48%)	2.79 ± 0.3 (11%)
	Hair-like subindividuals, thickness		21 ± 11 (53%)	
	Bubbles	22 ± 19 (86%)	14 ± 15 (107%)	2.3 ± 1.5 (65%)
II	Angular lumpy	716 ± 290 (49%)	471 ± 243 (89%)	1.49 ± 0.13 (9%)
	Bubbles	113 ± 74.6 (66%)	42.6 ± 15.9 (37%)	2.68 ± 1.54 (57%)
III	Horned	569 ± 155 (27%)	397 ± 70 (18%)	1.42 ± 0.14 (10%)
	Large bubbles	25 ± 2 (8%)	15 ± 9 (65%)	2.5 ± 1.9 (76%)
	Small bubbles	2.6 ± 1.25 (48%)	1.7 ± 1.14 (67%)	1.68 ± 0.37 (22%)
IV	Tabular	573 ± 346 (60%)	302 ± 177 (59%)	4.66 ± 4.15 (89%)

It should be emphasized that the above data on our tephra sample are well consistent with (Kyle and Jazek, 1978; Iverson et al., 2014) for ash from cores recovered at the Byrd station, Mary Byrd Land in the western Antarctic ice cover obtained at a height of 2154 m.

CHEMISTRY, TRACE ELEMENTS, AND LITHOGENIC GASES

The bulk chemical composition classifies the tephra under study as anorthoclase phonolite with a high positive correlation ($r = 0.61$) between the concentrations of Na_2O and K_2O (Table 2). The difference from the lava phonolite consists in a slightly higher alkalinity. Nevertheless, the tephra fairly well fits the general lineage of crystallization differentiation for Erebus lavas (Fig. 5). An analysis of the glass phase in the tephra showed that it is much less acidic compared with the bulk composition, varying in the following sequence: acid phonolites → alkali trachytes → trachytes → trachyrhyodacites → trachydacites → trachyrhyolites. In addition, there are occasional cases of a trachyandesitic glass phase. We thus see that the tephra differentiates into a glass phase that is more acidic than phonolite as a whole and a microlite feldspar fraction.

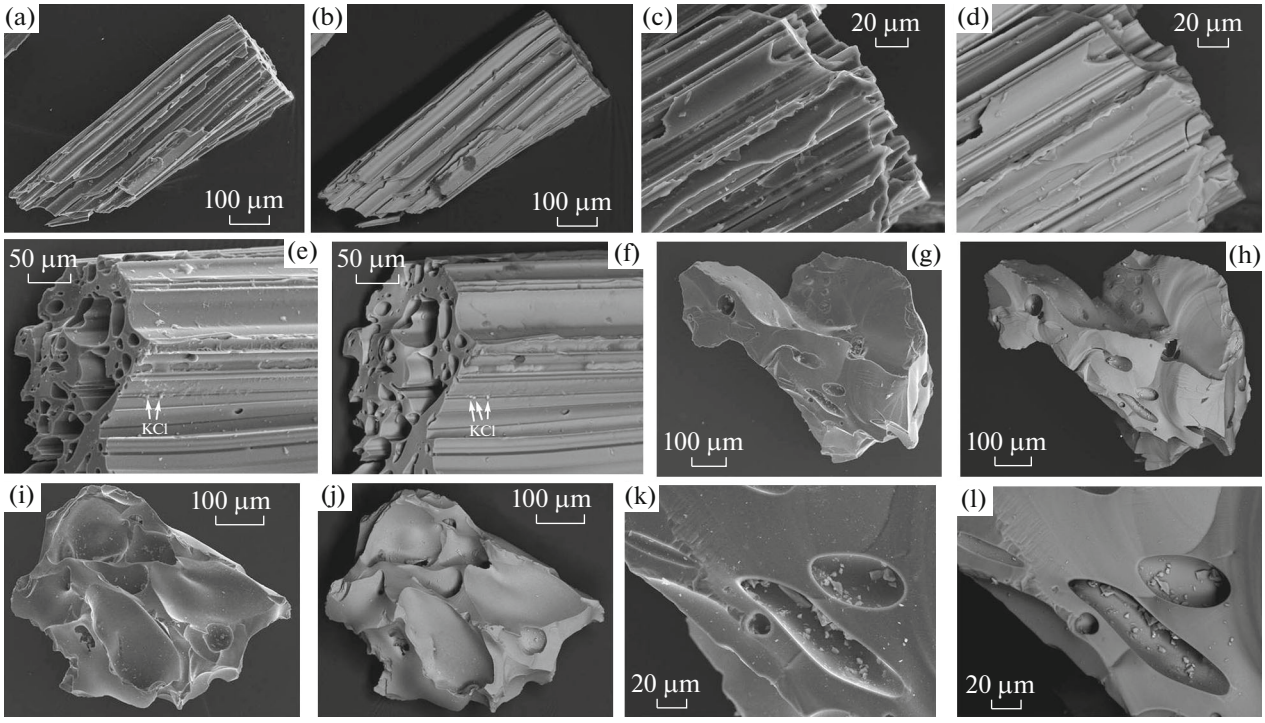

Fig. 3. Particles, subprismatic (a–f) and angular lumpy (g–l) with signs of microvesicularity. SEM images in secondary (a, c, e, g, i, k) and elastically reflected (b, d, f, h, j, l) electrons.

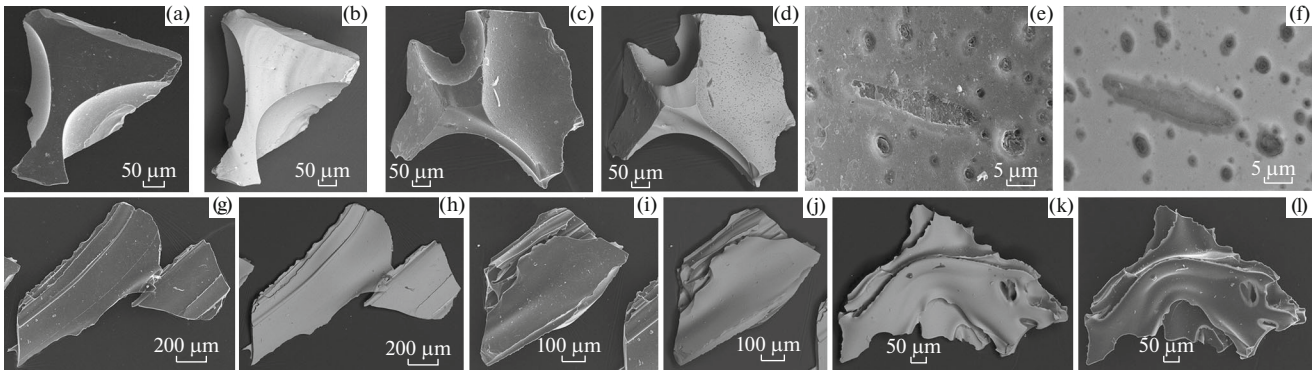

Fig. 4. Particles, horned (a–f) and tabular (g–l). SEM images in secondary (a, c, e, g, i, l) and in elastically reflected (b, d, f, h, j, k) electrons.

The tephra was found to contain 51 trace elements, including 14 lanthanoids (Table 3). The total concentration of trace elements ranges in the interval 3765–4425 g/t, with the total lanthanoids making 626 ± 106 g/t. The list of trace elements in this tephra is similar to that for the Erebus lava vulcanites, which demonstrate a smooth and continuous growth in the concentrations and varying proportions in favor of alkaline, alkaline earth, and rare earth elements in the direction from basanites to phonolites (Kelly et al., 2007). The average total trace elements for the tephra are approximately that for lava phonolites, but are greater than those for basanites, phonotephrites–tephrophonolites, and trachytes by factors of 1.34, 1.23, 1.43, respectively. The total lanthanoids for the tephra are greater than those for basanites, phonotephrites, and tephriphonolites by factors of 1.6, and 1.3 for lava phonolites. The trend of the chondrite-normalized lanthanoid concentrations in the tephra is overall similar to that in the lavas from basanites to phonolites, but is different in having a small Eu-minimum at the tephra curves. The spider-diagram for the tephra shows a deficit in basaltoid-compatible Sr and, on the contrary, a considerable excess in incompatible elements (Rb, Zr, Y, Th, and U), as well as in heavy lanthanoids (Fig. 6). The data point of tephra composition when plotted in the Th–Hf–Ta diagram (Wood, 1980) and in the Ta/Yb–Th/Yb diagram (Boynton, 1984), as well as in the Zr–Zr/Y diagram, definitely occurs in the fields of intraplate geodynamic settings.

Viewed from the standpoint of Yu.G. Shcherbakov's geochemical differentiation (Shcherbakov, 1965, 1976, 1982), the Erebus lava lineage shows a strong and orderly trend in the direction from basanites to phonolites as concerns increasing concentrations of centrifugal and deficit-centrifugal elements that compensates the loss in the concentration of centripetal and low-centrifugal elements. This is a definite confirmation of the Erebus lineage being due to the same process of magmatic differentiation. Viewed upon this background, the lava trachytes show contradictory properties. The concentrations of centrifugal and low-centrifugal elements in them are like those in phonotephrites and tephriphonolites, while the concentrations of centripetal and low-centrifugal elements makes them similar to phonolites. This is not entirely unexpected, being in agreement with the earlier inferences of American volcanologists as to a specific origin of trachytes on Erebus.

A mass occurrence of degassed bubbles in the microsculpture of tephra particles provides evidence of a considerable amount of gas in the primary melt. Our analysis revealed a broad association of components in the lithogenic gas phase, including both inorganic gases and a multitude of hydrocarbons in the range of C_1–C_4 alkanes and alkenes (Table 4). Judging from experimental data of (Iacovino et al., 2013), the Erebus lavas do absorb considerable amounts of volcanic gases, but this ability rapidly decreases with decreasing pressure, already in the range 700–400 MPa. It is in the lava phonotephrites that the concentration of dissolved gases becomes the lowest, approximately at the level 0.2–0.3% for H_2O and 0.05–0.2% for CO_2, which is nearly identical with our data for the tephra, namely, approximately 0.15% for H_2O and 0.02% for ($CO + CO_2$). The slightly lower concentrations of gas in our tephra seem to be a signature of its explosive origin.

From the viewpoint of petrology, the composition of lithogenic gases identified in the Erebus tephra correlates with that in products of crust–mantle interaction, being much nearer to mantle formations proper. This is indicated by a considerable amount of carbon monoxide in the pyrolysate (Fig. 7a) and by the dominance of C_2–C_4 hydrocarbons over methane (see Fig. 7b). In addition, the Erebus tephra has the composition of hydrocarbons in the pyrolysate similar to the basaltic andesite lavas discharged during the Tolbachik eruption of 2012–2013 (see Fig. 7c), thus providing evidence that the composition of lithogenic gases in volcanic ejecta is controlled by the depth at which the material source resides rather than by the composition and facies nature of the ejecta.

Table 2. The bulk chemical composition of ash (1) and the chemical composition of the glass phase contained therein (2–33), wt %

##	SiO_2	TiO_2	ZrO_2	Al_2O_3	Fe_2O_3	Y_2O_3	ZnO	MnO	MgO
1	52.25	0.78	0.17	21.45	6.07	0.01	0.02	0.31	1.06
2	58.20	1.05	N. f.	18.51	5.87	N. f.	N. f.	0.38	N. f.
3	59.03	1.15	″	17.72	6.27	″	″	N. f.	″
4	61.41	1.09	″	17.28	5.93	″	″	0.40	″
5	64.53	0.94	″	15.01	5.55	″	″	0.45	″
6	58.31	1.57	″	17.76	7.18	″	″		″
7	64.76	1.10	″	10.81	5.75	″	″		″
8	70.30	1.19	″	11.52	3.99	″	″	0.37	″
9	74.96	1.14	″	9.91	3.53	″	″	0.47	″
10	75.40	1.42	″	8.69	3.90	″	″	N. f.	″
11	56.84	1.08	″	17.2	6.66	″	″	0.41	″
12	57.13	1.10	″	18.61	7.56	″	″	N. f.	″
13	57.92	1.11	″	17.86	7.46	″	″	″	″
14	59.55	1.35	″	17.50	6.04	″	″	″	″
15	71.77	1.32	″	7.84	7.67	″	″	″	″
16	85.98	1.36	″	4.98	4.08	″	″	″	″
17	86.56	1.63	″	4.23	3.98	″	″	0.41	″
18	59.51	1.36	″	16.58	8.45	″	″	N. f.	″
19	57.26	1.38	″	17.75	7.12	″	″		″
20	57.18	1.18	″	17.89	7.66	″	″	0.51	″
21	58.43	1.21	″	18.24	6.63	″	″	0.39	″
22	57.76	1.22	″	18.89	6.82	″	″	0.55	″
23	57.94	0.92	″	17.35	6.39	″	″	N. f.	″
24	58.22	1.10	″	18.16	7.09	″	″	″	″
25	58.12	1.29	″	17.92	7.74	″	″	″	″
26	58.75	1.26	″	17.75	6.95	″	″	0.48	″
27	59.55	1.30	″	19.36	6.36	″	″	N. f.	″
28	57.26	1.66	″	17.75	8.09	″	″	″	″
29	56.51	1.41	″	16.99	7.76	″	″	″	″
30	62.63	1.14	″	14.53	6.0	″	″	″	″
31	62.73	1.44	″	13.65	5.93	″	″	0.44	″
32	59.14	1.50	″	16.85	7.63	″	″	0.43	″
33	58.48	1.03	″	18.14	6.86	″	″	N. f.	″

Table 2. (Contd.)

##	CaO	SrO	Na_2O	K_2O	Rb_2O	Nb_2O_5	P_2O_5	SO_3	Cl
1	2.88	0.02	7.08	7.19	0.35	0.28	0.35	0.28	N. f.
2	1.94	N. f.	8.51	5.29	N. f.	N. f.	N. f.	N. f.	0.25
3	1.90	″	7.57	6.36	″	″	″	″	N. f.
4	1.85	″	6.50	5.54	″	″	″	″	
5	1.70	″	6.66	4.92	″	″	″	″	0.24
6	2.02	″	6.94	6.22	″	″	″	″	N. f.
7	2.22	″	9.66	5.44	″	″	″	″	0.26
8	1.66	″	5.47	4.20	″	″	″	1.02	0.28
9	1.31	″	4.90	3.48	″	″	″	N. f.	0.30
10	1.12	″	5.21	3.32	″	″	″	0.62	0.32
11	2.06	″	9.08	5.76	″	″	0.72	N. f.	0.19
12	1.96	″	7.56	5.80	″	″	N. f.	″	0.28
13	2.15	″	7.04	6.22	″	″	″	″	0.24
14	1.79	″	7.79	5.98	″	″	″	″	N. f.
15	3.57	″	3.69	2.40	″	″	″	1.43	0.31
16	0.50	″	N. f.	1.97	″	″	″	0.60	0.53
17	0.41	″	″	1.58	″	″	″	0.69	0.51
18	1.84	″	5.91	6.35	″	″	″	N. f.	N. f.
19	2.13	″	7.51	6.29	″	″	″	0.27	0.29
20	2.26	″	6.73	6.59	″	″	″	N. f.	N. f.
21	2.04	″	7.05	5.73	″	″	″	″	0.28
22	2.12	″	6.71	5.93	″	″	″	″	
23	2.37	″	8.77	6.05	″	″	″	″	0.21
24	2.17	″	6.53	6.47	″	″	″	″	0.26
25	2.28	″	6.15	6.50	″	″	″	″	N. f.
26	1.80	″	6.57	6.18	″	″	″	″	0.26
27	1.83	″	6.83	5.46	″	″	″	″	N. f.
28	2.23	″	6.24	6.53	″	″	″	″	0.24
29	2.07	″	2.07	6.81	″	″	″	″	N. f.
30	1.65	″	9.08	4.97	″	″	″	″	″
31	2.39	″	6.36	5.32	″	″	″	1.42	0.32
32	1.91	″	5.51	7.03	″	″	″	N. f.	N. f.
33	1.76	″	7.24	6.49	″	″	″	″	″

The analyses have been converted to 100%; N. f. stands for Not found.

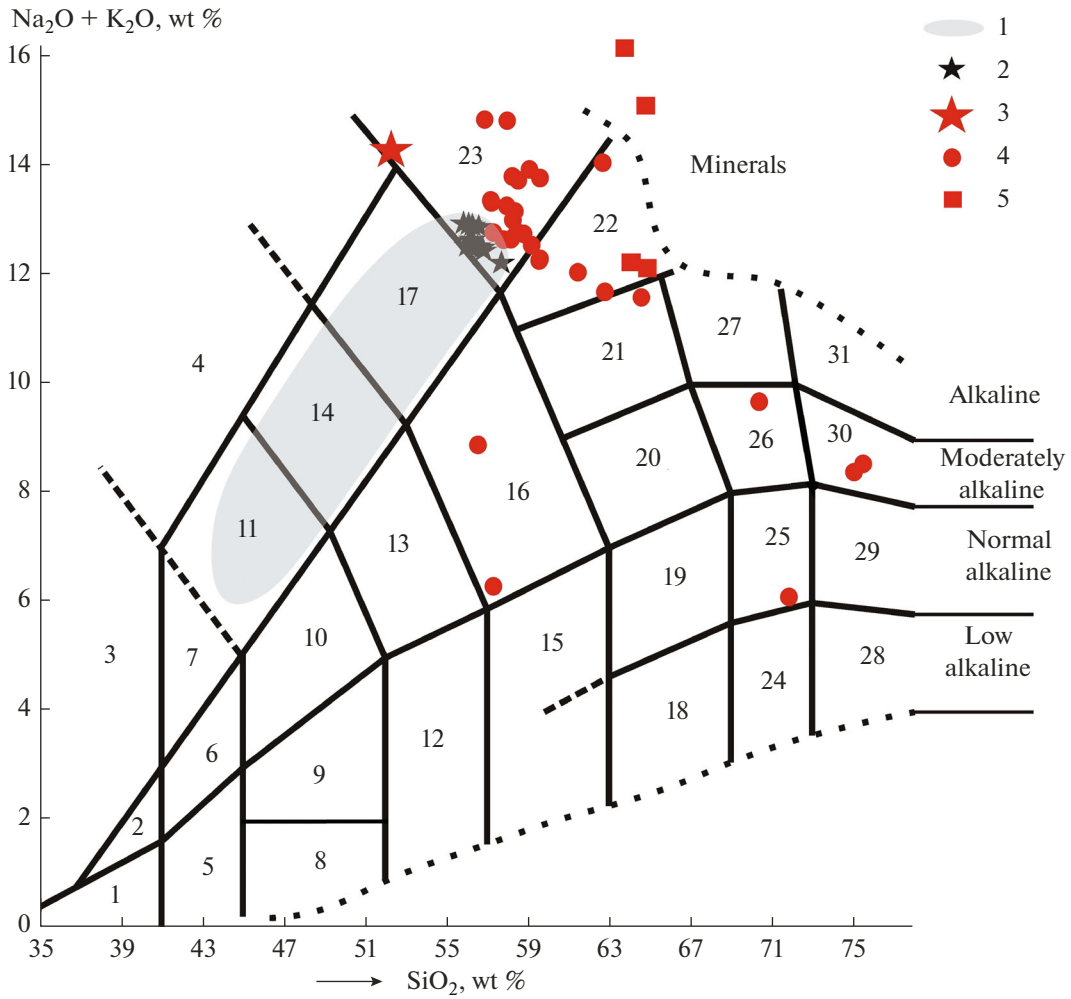

Fig. 5. A TAS diagram (*Petraficheskii kodeks ...,* 2008) illustrating the chemistry of ejecta discharged as the effusive and explosive facies by Mount Erebus. The fields in the diagram: (1) picrites; (2, 3) picrites, moderately alkaline and alkaline, respectively; (4) fondites; (5–8) picrobasalts: ultrabasic, moderately alkaline, alkaline, and basic, respectively; (9) basalts; (10) trachybasalts; (11) alkaline basalts; (12) basaltic andesites; (13) basaltic trachyandesites; (14) phonotephrites; (15) andesites; (16) trachyandesites; (17) tephriphonolites; (18) low-alkali dacites; (19) dacites; (20) trachydacites; (21) trachytes; (22) alkaline trachytes; (23) phonolites; (24) low-alkali rhyodacites; (25) trachydacites; (26) trachyrhyodacites; (27) alkali rhyodacites (pantellerite); (28) low-alkali rhyolites; (29) rhyolites; (30) trachyrhyolites; (31) alkali rhyolites (comendites). Objects of study: (1) lavas in the general Erebus lineage; (2) lava phonolites; (3–5) data on our tephra sample: bulk composition, glass phase in particles, and feldspar microlites, respectively.

MINERAL AND PHASE COMPOSITION

An X-ray diffractogram of the Erebus tephra shows a wide radiation band (FWHM = 11°) in the angle range 2Θ 22°–37° whose maximum occurs at 26.7°, which corresponds to $d/n = 3.3$ Å. This must be volcanic glass. Two narrow reflexes are observed in the region of extremum for the band, 3.34 and 3.22 Å, indicating an insignificant admixture of quartz and feldspar, respectively. The X-ray data thus show, when combined with analytic SEM results, that the tephra largely consists of intermediate to acidic glass. The insignificant admixture includes numerous microminerals like oxygen salts, magnetite, rutile, pyrite, native metals, and chlorides, aside from feldspars and quartz. All of these minerals make a paragenesis that is very typical of exactly the explosive facies of Cenozoic volcanism (Karpov et al., 2017).

The feldspars in this tephra (Table 5) are occasional Ca-bearing orthoclase and a definitely dominant anorthoclase having the composition $(Na_{0.61–0.69}K_{0.24–0.31}Ca_{0.06–0.08})[Al_{0.89–0.92}Fe_{0.15–0.18}O_8]$. Regarded in its endmember composition, the latter mineral is anorthite–orthoclase–albite (mol %): albite 60–70, orthoclase 25–30, and anorthite 3–8, which is in complete agreement with the region of complete miscibility for the endmembers. It is a known fact (Kelly et al., 2007) that the anorthoclase that is present in lavas has a much more variable composition: one has

Table 3. Trace elements in the Erebus tephra and lavas, g/t

Elements	Tephra					Lavas			
	1	2	3	4	Mean ± RMSE	5	6	7	8
Li	17	31	28	30	26.5 ± 6.455	Not determ.	Not determ.	Not determ.	Not determ.
Rb	260	140	138	141	169.75 ± 60.179	40.333 ± 0.577	70.4 ± 11.442	102.8 ± 3.194	146.5 ± 20.506
Tl	0.5	Not detected.	Not detected	Not detected	Not determ.	Not determ.	Not determ.	Not determ.	Not determ.
Cs	1.3	1.6	1.79	1.93	1.655 ± 0.273	0.393 ± 0.012	0.696 ± 0.149	1.22 ± 0.102	2.815 ± 1.237
Be	5.4	10	10	11	9.1 ± 2.51	Not determ.	Not determ.	Not determ.	Not determ.
Sr	230	279	261	253	255.75 ± 20.32	1286.667 ± 161.769	1157.7 ± 185.796	869.6 ± 87.928	47 ± 48.043
Ba	310	500	460	449	429.75 ± 82.786	606.667 ± 106.359	820.7 ± 154.726	1086.4 ± 65.198	557.5 ± 358.503
Co	21	2	2	2.3	6.825 ± 9.451	Not determ.	Not determ.	Not determ.	Not determ.
Ni	2	Not detected	Not detected	Not detected	Not determ.	28.667 ± 29.771	10.2 ± 6.529	7 ± 1.225	8 ± 1.414
Cu	6	″	″	″	1.5 ± 3	29.333 ± 11.846	25.7 ± 15.355	10.6 ± 1.342	8.5 ± 0.707
Zn	90	173	160	167	147.5 ± 39	109.667 ± 4.933	113.8 ± 15.411	128.4 ± 24.724	222.5 ± 65.76
Pb	4	14	6	7	7.75 ± 4.349	3.5 ± 0.5	3.7 ± 0.949	3.9 ± 0.742	23.5 ± 10.607
Cd	0.5	Not detected	Not detected	Not detected	Not determ.	Not determ.	Not determ.	Not determ.	Not determ.
Sn	5	″	″	″	0.125 ± 0.25	″	″	″	″
Mo	19	″	″	″	4.75 ± 9.5	″	″	″	″
Ag	8	″	″	″	2 ± 4	″	″	″	″
Y	70	66	76	83	73.75 ± 7.411	40.667 ± 3.512	44.9 ± 5.131	59.2 ± 7.463	81.5 ± 44.849
Zr	1600	1419	1592	1580	1547.75 ± 86.226	356 ± 8.185	568.7 ± 104.045	921 ± 37.596	1027 ± 82.024
Nb	390	362	414	407	393.25 ± 23.143	122.667 ± 10.408	175.9 ± 20.475	251.6 ± 10.237	245 ± 18.385
Ga	23	33	31	34	30.25 ± 4.992	21.333 ± 0.577	23.8 ± 1.317	28 ± 0.707	32 ± 1.414
Ge	0.8	Not detected	Not detected	Not detected	Not determ.	Not determ.	Not determ.	Not determ.	Not determ.
Sc	3.5	″	5	4.9	3.35 ± 2.336	14.2 ± 5.283	6.452 ± 3.363	3.272 ± 0.93	4.13 ± 1.895
V	5	″	2	2.4	2.35 ± 2.055	220.667 ± 61.256	69.3 ± 49.867	18 ± 10	9 ± 1.414
Cr	0.2	″	Not detected	Not detected	Not determ.	55.333 ± 65.286	13.25 ± 20.291	2.3 ± 0.447	1.5 ± 0.707
Hf	20	2.95	31.3	30.8	21.263 ± 13.275	8.003 ± 0.435	11.94 ± 2.582	20.2 ± 1.134	23.35 ± 2.616
Ta	15	21.4	23.1	23.1	20.65 ± 3.851	7.13 ± 0.493	10.263 ± 1.319	14.7 ± 0.561	13.55 ±1.485
W	3.2	Not detected	Not detected	Not detected	Not determ.	Not determ.	Not determ.	Not determ.	Not determ.

Table 3. (Contd.)

Elements	Tephra					Lavas			
	1	2	3	4	Mean ± RMSE	5	6	7	8
Th	19.6	27.5	29.8	30.4	26.825 ± 4.98	6.967 ± 0.321	12.39 ± 2.088	18.46 ± 0.673	23.4 ± 2.828
U	6	7.3	8.8	9.1	7.8 ± 1.435	1.833 ± 0.208	3.62 ± 0.987	5.54 ± 0.684	7.4 ± 0.707
La	110	161	153	166	147.5 ± 25.567	75.433 ± 4.844	99.59 ± 12.095	119.02 ± 12.515	148.55 ± 23.122
Ce	220	304	294	319	282 ± 41.857	161.467 ± 10.484	203.25 ± 22.887	248.22 ± 27.437	296.75 ± 40.093
Pr	22	33	32	34	30.25 ± 5.56	Not determ.	Not determ.	Not determ.	Not determ.
Nd	70	109	103	113	98.75 ± 19.62	76 ± 9	87.3 ± 11.567	95.4 ± 13.465	127 ± 25.456
Sm	12	17.8	17.7	19.3	16.7 ± 3.218	13.393 ± 0.82	55.619 ± 88.293	14.628 ± 2.107	19.015 ± 2.807
Eu	2.4	3.71	3.56	3.72	3.347 ± 0.636	3.94 ± 0.27	3.922 ± 0.412	4.69 ± 0.429	3.135 ± 0.318
Gd	11	13.05	13.56	15.4	13.252 ± 1.809	″	″	″	″
Tb	1.4	2.1	2.24	2.45	2.047 ± 0.455	1.483 ± 0.133	1.58 ± 0.199	1.882 ± 0.24	2.525 ± 0.488
Dy	9	12.7	12.7	13.8	12.05 ± 2.098	Not determ.	Not determ.	Not determ.	Not determ.
Ho	1.7	2.52	2.56	2.75	2.387 ± 0.456	″	″	″	″
Er	5	7.2	7.39	7.76	6.831 ± 1.247	″	″	″	″
Tm	0.7	1.1	1.13	1.19	1.03 ± 0.223	″	″	″	″
Yb	4.8	7.3	7.16	7.4	6.66 ± 1.24	2.86 ± 0.31	3.593 ± 0.576	5.352 ± 0.524	7.095 ± 1.11
Lu	0.7	1.11	1.12	1.15	2.595 ± 2.937	0.44 ± 0.04	0.533 ± 0.81	0.808 ± 0.006	1.05 ± 0.17
P	800	Not detected	Not detected	Not detected	Not determ.	Not determ.	Not determ.	Not determ.	Not determ.
S	0.8	″	″	″	″	″	″	″	″
Te	1.8	″	″	″	″	″	″	″	″
As	6.2	″	″	″	″	0.833 ± 0.289	1.35 ± 0.412	1.1 ± 0.0548	2.85 ± 1.343
Se	0.9	″	″	″	″	Not determ.	Not determ.	Not determ.	Not determ.
Sb	0.4	″	″	″	″	0.067 ± 0.029	0.14 ± 0.084	0.27 ± 0.045	0.4 ± 0.141
Bi	0.009	″	″	″	″	Not determ.	Not determ.	Not determ.	Not determ.
B	8	″	″	″	″	″	″	″	″

Determinations were carried out using the solution method with subsequent ICP-MS. Analyses: (1) *Geoanalitik* TsKP UrB RAS, Yekaterinburg; (2–4) Arkansas State University, U.S. Concentrations are given as mean ± rms error. The data on lavas were borrowed from (Kyle et al., 1992), (5–8) basanites, phonotephrites and tephriphonolites, orthoclase phonolites, and trachytes, respectively.

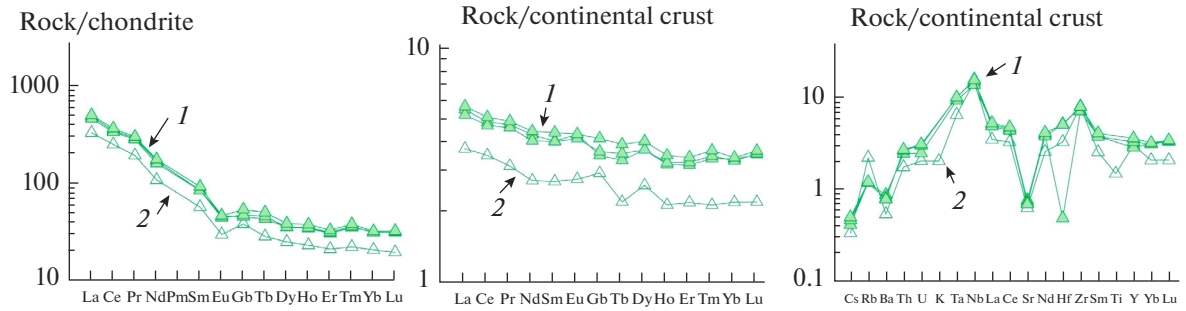

Fig. 6. The normalized concentrations of trace elements in the tephra sample. (1) after (Kyle et al., 1992); (2) according to this study.

orthoclase–albite–anorthite in basanites and anorthite–orthoclase–albite in phonolites, but anorthite is much more abundant (up to 23 mol %) there than in the tephra phonolite.

Zircon in the tephra was found in the glass in the form of occasional inclusions, frequently as pyramidal prismatic crystals (typical of zircon) (6.9 ± 7.4) × (3.7 ± 2.7) μm in size (Figs. 8a, 8b). The composition of this zircon (Table 6) was found using the formula $(Zr_{0.97–0.99}Hf_{0–0.01})[SiO_4]$.

The phosphate group includes apatite and monazite. The former mineral is *chlorohydroxylapatite* having the composition $(Ca_{9.75–10.06}Sr_{0–0.35}Mn_{0–0.21})_{9.89–10.06}[P_{5.64}S_{0–0.36}O_{24}](OH)_{1.66–2.34}Cl_{0–0.59}$ and releasing minute, mostly oval, exhalations (0.9 ± 0.6) × (0.14 ± 0.21) μm in size (see Figs. 8c, 8d). The other phosphate in the tephra is *La-Ce-Nd monazite*; it is encountered in growths with rutile and orthoclase as isometric grains (5–7) × (3–4) μm in size (see Figs. 8e, 8f).

The Sr-bearing barite of the composition $(Ba_{0.93–0.95}Sr_{0.05–0.07})[SO_4]$ mostly occurs as homogeneous grains of irregular shapes (4.34 ± 1.45) × (3.4 ± 1.85) μm in size. Some barite grains have an aggregate structure, consisting of numerous tightly coalesced subindividuals of angular oval shapes and being (0.51 ± 0.38) × (0.13 ± 0.05) μm in size.

Magnetite occurs in tephra rather frequently and in various forms, ranging between flaky accumulations of mesonanometer particles (Figs. 9a, 9b) and isolated grains (2.01 ± 2.9) × (1.39 ± 1.87) μm in size (see Figs. 9c, 9d). There are occasional grains 6–8 μm across that show nanoporosity (see Figs. 9e, 9f). The composition of the mineral (Table 7) is described by the formula $(Fe_{0.94–1}Mn_{0–0.06})(Fe_{1.28–1.99}Ti_{0–0.64}Al_{0–0.29})_2O_4$. Compositional calculations for endmembers leads one to the conclusion that the tephra contains four varieties of magnetite, namely (in the order of decreasing frequency of occurrence), hercynite-magnetite, magnetite, ulvite-magnetite, and magnetite-ulvite.

Table 4. The composition of gas pyrolysates obtained by heating the Erebus tephra sample

Components	Heating up to 400°C	Heating in the range 400–1000°C	Total
N_2	Not detected	24.41/1.39	24.41/0.45
H_2O	3569/98.179	1479/84.18	5048/93.56
CO_2	66.11/1.819	181.64/10.32	247.75/4.59
CO	Not detected	38.96/2.21	38.96/0.72
CH_4	0.082/0.002	14.09/0.8	14.172/0.26
C_2H_4	Not detected	8.77/0.5	8.77/0.16
C_2H_6	"	2.67/0.15	2.67/0.05
C_3H_6	"	6.58/0.37	6.58/0.12
C_3H_8	"	1.72/0.1	1.72/0.03
C_4H_8	"	1.10/0.06	1.10/0.02
nC_4O_{10}	"	0.21/0.01	0.21/0.004
iC_4O_{10}	"	1.04/0.06	1.04/0.02
Сумма	3635.192/100	1760.19/100	5395.382/100

Gas concentrations in pyrolysate: in g/t in front of the slash and in wt % after the slash.

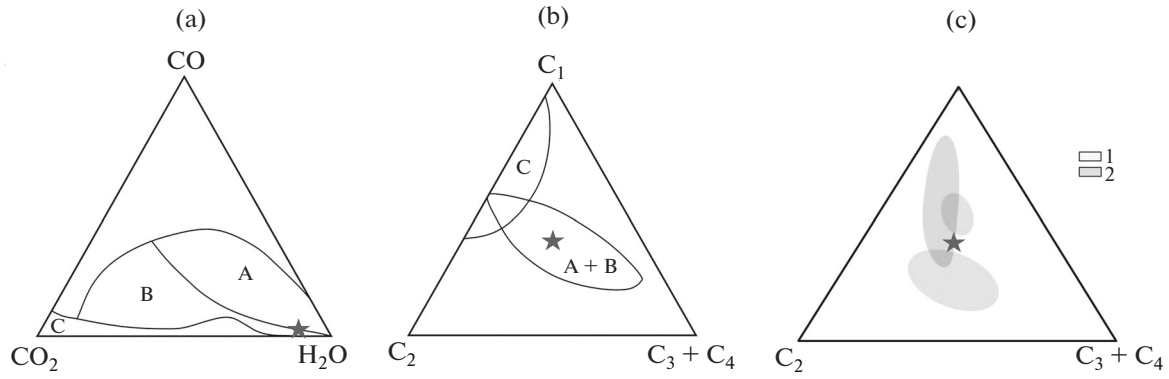

Fig. 7. Petrologic aspects in the origin of lithogenic gases in the Erebus tephra. (a) proportions of inorganic gases in mantle–crust derivates (A stands for mantle derivates (diamonds), B for products of mantle–crust interactions (minerals in diamond-bearing parastereseis), C stands for crustal derivates (Petrovsky et al., 2008); (b) same for hydrocarbon gases; (c) proportions of hydrocarbon gases in pyrolysates obtained by heating TFE-50 lavas to a temperature of 400°C (1) and in the range 400–1000°C (Silaev et al., 2019) (2). Star shows the composition of lithogenic gases in the tephra.

One characteristic admixture in the tephra consists in the presence of numerous inclusions of native metals (3.9 ± 1.9) × (1.9 ± 1) μm in size whose elongation index is 2.2 ± 0.8 (Fig. 10). The inclusions are dominated by *brass* of the composition $Cu_{0.55–0.59}Zn_{0.37–0.4}Fe_{0.02–0.06}Pb_{0–0.01}$ (Table 8). In addition to brass, one occasionally encounters Cu-Fe-bearing *native tin*. It should be emphasized that native-metal mineralization is rather characteristic chiefly of the explosive volcanic facies (Karpov et al., 2017). Special importance attaches to the detection of isometric *chloride* particles in the tephra (see Figs. 3e, 3f), which frequently occur near degassing-induced bubbles. The particles vary in size in the range (3.5 ± 1.57) × (2.7 ± 1) μm. Judging from the composition, these are sylvite solid solutions (see Table 8): (0.77–0.8) KCl + (0.17–0.2) NaCl + 0.03 $CaCl_2$.

It should be emphasized that the explosive phonolite under study here has not been found to contain nepheline whose presence in the Erebus effusive tephriphonolites and phonolites was previously noted by American volcanologists. It is possible that the sample was too small and contained too much glass.

CARBONACEOUS MATERIAL

The fact of hydrocarbons being detected in the lithogenic gases from the Erebus tephra provides evidence that condensed carbonaceous material may be present in the tephra. Coulometric titration based on the value of pH (An-7529M) showed that the bulk concentration of carbon in the sample under study varied in the range 0.02–0.05 wt %, which is an order of magnitude greater than that of hydrocarbon gases in the tephra. It follows that the Erebus tephra is dominated by an admixture of nongaseous carbonaceous components. An isotope analysis of this component (6 determinations) resulted in the following value of the isotope ratio: $\delta^{13}C_{PDB} = -26.47 \pm 0.34‰$. This result lies within our earlier data for the so-called atomic dispersed form of carbon (Haggerty, 1999) on present-day volcanoes of Kamchatka and the Pacific

Table 5. The chemical (wt %) and the endmember(mol %) compositions of feldspars

##	SiO_2	Al_2O_3	Fe_2O_3	CaO	Na_2O	K_2O	Empirical formulas	Endmembers		
								Albite	Anorthite	Orthoclase
1	64.96	17.23	4.36	1.33	7.94	4.18	$(Na_{0.69}K_{0.24}Ca_{0.06})_{0.99}$ $[Al_{0.92}Fe_{0.15}Si_{2.94}O_8]$	70	6	24
2	64.95	17.23	4.36	1.33	7.94	4.19	$(Na_{0.69}K_{0.24}Ca_{0.06})_{0.99}$ $[Al_{0.92}Fe_{0.15}Si_{2.93}O_8]$	68.8	6.4	24.8
3	64.09	16.67	5.37	1.61	6.94	5.32	$(Na_{0.61}K_{0.31}Ca_{0.08})$ $[Al_{0.89}Fe_{0.18}Si_{2.93}O_8]$	61.2	7.8	31
4	63.80	18.61	0.60	0.75	N. f.	16.24	$(K_{0.96}Ca_{0.04})$ $[Al_{1.02}Fe_{0.02}Si_{2.96}O_8]$	None	3.7	96.3

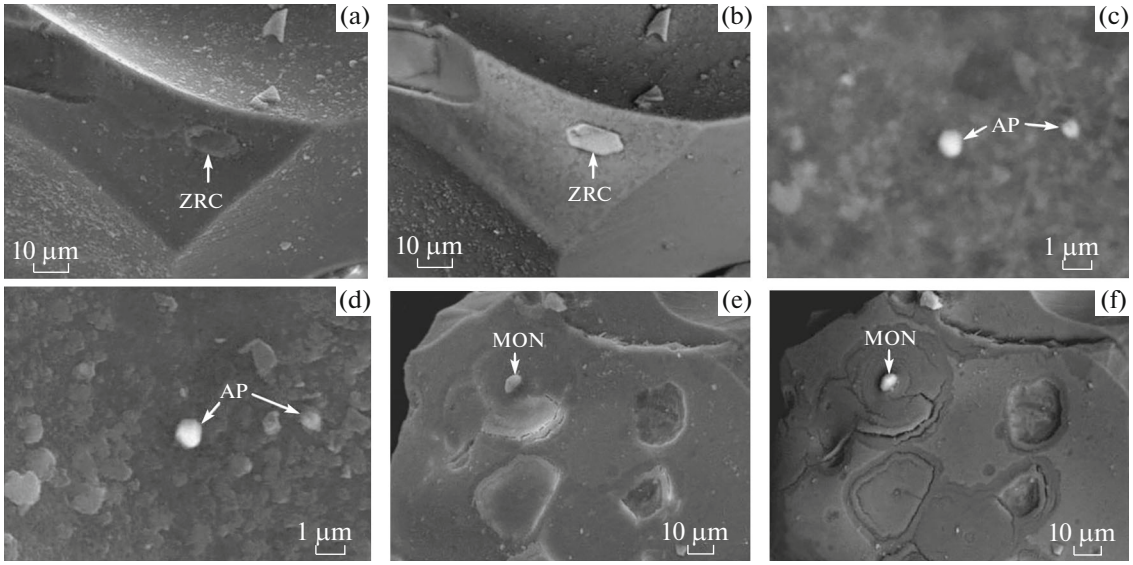

Fig. 8. Exhalations of accessory silicates and phosphates in the tephra. Minerals: ZRC zircon, AP apatite, MON monazite. SEM images in secondary (a, c, e) and in elastically reflected (b, d, f) electrons

Ring of Fire, as well as for organoids of volcanogenic atmospheric electrogenic origin (Silaev et al., 2016, 2018).

CONCLUSIONS

First multidisciplinary petrologic, mineralogical, and geochemical studies were carried out on tephra sampled from the greatest intraplate Erebus stratovolcano, Antarctica, which has a unique basanite–phonolite effusive lineage. The sample consists of angular lumpy, prismatic, horned, and tabular particles that vary widely in size between 0.3 × 0.1 and 2 × 0.7 mm. There are two characteristic features of the particles, namely, their microvesicularity and shape elongation, giving elongation indices between 1.2 and 8. Obviously enough, this habitus is due to the explosive origin of the tephra. The tephra bulk chemical composition classifies it as an anorthoclase phonolite that has slightly greater alkalinity than lava phonolites. With regard to its phase composition, the tephra largely consists of volcanic glass that shows a widely varying chemical composition, from phonolite to trachyrhyolite.

The sample was found to contain 51 trace elements whose total concentration varies in the range 3765–

Table 6. The composition of zircon (1–3), apatite (4–10), and barite (11, 12)

##	SiO_2	ZrO_2	HfO_2	MnO	CaO	BaO	SrO	P_2O_5	SO_3	Cl	Empirical formulas
1	32.59	65.78	1.63	N. f.	N. f.	N. f.	N. f.	N. f.	N. f.		$(Zr_{0.98}Hf_{0.01})_{0.99}[SiO_4]$
2	33.06	66.94	N. f.	″	″	″	″	″	″		$Zr_{0.99}[SiO_4]$
3	33.54	66.46	″	″	″	″	″	″	″		$Zr_{0.97}[SiO_4]$
4	N. f.	N. f.	″	″	56.14	″	″	42.80	″	4.06	$Ca_{9.98}[P_6O_{24}](OH)_{1.96}Cl_{0.3}$
5	N. f.	″	″	″	56.37	″	″	43.36	″	0.27	$Ca_{9.89}[P_6O_{24}](OH)_{1.7}Cl_{0.07}$
6	N. f.	″	″	″	53.0	″	3.56	40.35	1.05	2.04	$(Ca_{9.75}Sr_{0.35})_{10.1}[P_{5.86}\ S_{0.14}O_{24}]OH)_{1.75}Cl_{0.59}$
7	N. f.	″	″	″	57.46	″	N. f.	42.54	N. f.	N. f.	$Ca_{10.06}[P_6O_{24}](OH)_{2.12}$
8	N. f.	″	″	″	56.72	″	″	43.01	″	0.27	$Ca_{10.03}\ [P_6O_{24}](OH)_{1.98}\ Cl_{0.08}$
9	N. f.	″	″	″	56.18	″	″	42.89	″	0.93	$Ca_{9.96}[P_6O_{24}](OH)_{1.66}Cl_{0.26}$
10	N. f.	″	″	1.37	49.39	″	″	46.65	2.59	N. f.	$(Ca_{9.78}Mn_{0.21})_{9.99}[P_{5.64}\ S_{0.36}O_{24}](OH)_{2.34}$
11	N. f.	″	″	N. f.	N. f.	61.98	3.22	N. f.	34.8	″	$(Ba_{0.93}Sr_{0.07})[SO_4]$
12	N. f.	″	″	″	″	62.14	3.16	″	34.7	″	$(Ba_{0.94}Sr_{0.07})[SO_4]$

N. f. stands for Not found.

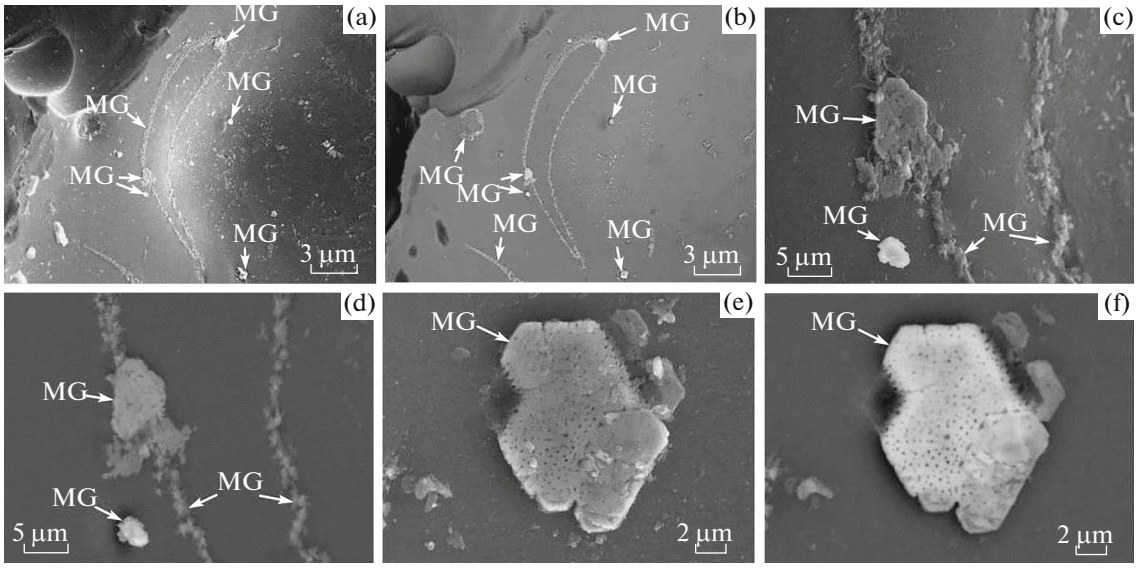

Fig. 9. Exhalations of magnetite varieties (MG) in the tephra. SEM images in secondary (a, c, e) and in elastically reflected (b, d, f) electrons.

4425 g/t, with the total lanthanoids being 626 ± 106 g/t. The mean total trace elements in this tephra make it very similar to lava phonolite, while exceeding basanite, phonotephrite–tephriphonolite, and trachytes by factors of 1.34, 1.23, and 1.43, respectively. Its total lanthanoids exceed basanite, phonotephrite, and tephriphonolite by a factor of 1.6 and lava phonolite by 1.3. Viewed within the theory of geochemical differentiation due to Yu.G. Shcherbakov, the tephra fairly well fits the common sequence of magmatic differentiation known as the Erebus lineage, but requires some correction for the explosive origin of the tephra. Several geochemical criteria identify this tephra as volcanic ejecta that were specifically formed in an intraplate geodynamic rift setting.

There were some admixtures to the volcanic glass in the tephra. These were identified and studied, including feldspars of the anorthite–orthoclase–albite and orthoclase compositions; fluochlorohydroxylapatite; La–Ce–Nd monazite; Sr-bearing barite; spinellids whose compositions vary from magnetite to hercynite-magnetite, ulvite-magnetite, and magnetite-ulvite; Fe–Pb-bearing brass, and Cu–Fe-bearing native tin; chloride solid solutions of the hydrophilite-halite-sylvite composition.

Table 7. The chemical (wt %) and the endmember (mol %) compositions of magnetite

##	Fe_2O_3	TiO_2	Al_2O_3	MnO	Empirical formulas	Endmembers			
						Magnetite	Ulvite	Hercynite	Jacobsite
1	74.88	21.6	1.16	1.86	$(Mn_{0.06}Fe_{0.94})(Fe_{1.28}Ti_{0.64}Al_{0.08})_2O_4$	26	64	4	6
2	98.34	0.74	N. f.	0.92	$(Mn_{0.03}Fe_{0.97})(Fe_{1.98}Ti_{0.02})O_4$	95	2	None	3
3	91.67	7.16	″	1.17	$(Mn_{0.04}Fe_{0.96})(Fe_{1.79}Ti_{0.21})_2O_4$	75	21	″	4
4	94.76	5.23	″	N. f.	$(Fe(Fe_{1.84}Ti_{0.16})_2O_4$	84	16	″	N. f.
5	98.85	0.4	0.75	″	$Fe(Fe_{1.95}Ti_{0.01}Al_{0.04})_2O_4$	97	1	2	″
6	92.65	0.84	6.51	″	$Fe(Fe_{1.6}Ti_{0.03}Al_{0.29})_2O_4$	82.5	3	14.5	″
7	97.82	N. f.	2.18	″	$Fe(Fe_{1.99}Al_{0.01})_2O_4$	99.5	None	0.5	″
8	94.85	″	5.15	″	$Fe(Fe_{1.75}Al_{0.25})_2O_4$	87.5	″	12.5	″
9	96.49	″	3.51	″	$Fe(Fe_{1.81}Al_{0.19})_2O_4$	90.5	″	9.5	″
10	97.27	″	2.72	″	$Fe(Fe_{1.87}Al_{0.13})_2O_4$	93.5	″	6.5	″

N. f. stands for Not found

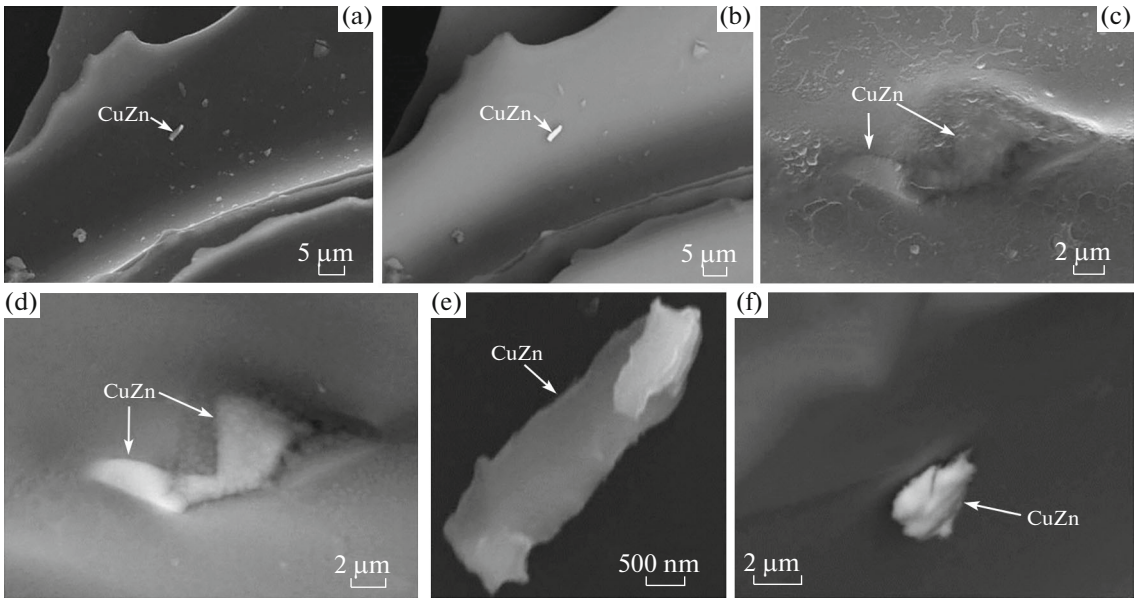

Fig. 10. Exhalations of native brass (CuZn) in the tephra. SEM images in secondary (a, c) and in elastically reflected (b, d–f) electrons.

Table 8. The chemical composition of chloride solid solutions and metal alloys, wt %

##	Na	K	Ca	Cl	Cu	Zn	Sn	Pb	Fe	Ni	Empirical formulas
1	5.61	25.72	1.31	49.38	N.f.	N.f.	N.f.	N.f.	N.f.	N. f.	$0.8KCl + 0.17NaCl + 0.03CaCl_2$
2	6.47	42.45	1.14	49.94	″	″	″	″	″	″	$0.77KCl + 0.2NaCl + 0.03CaCl_2$
3	Not detected	Not detected	Not detected	Not detected	55.99	38.33	N. f.	3.59	2.09	N. f.	$Cu_{0.58}Zn_{0.39}Fe_{0.02}Pb_{0.01}$
4	″	″	″	″	56.53	37.44	″	0.94	5.09	″	$Cu_{0.57}Zn_{0.37}Fe_{0.06}$
5	″	″	″	″	54.88	41.96	″	N. f.	3.16	″	$Cu_{0.55}Zn_{0.41}Fe_{0.04}$
6	″	″	″	″	55.12	41.20	″	″	3.68	″	$Cu_{0.55}Zn_{0.39}Fe_{0.02}Pb_{0.01}$
7	″	″	″	″	59.36	38.25	″	″	2.39	″	$Cu_{0.58}Zn_{0.40}Fe_{0.05}$
8	″	″	″	″	57.60	38.04	″	1.74	1.55	1.07	$Cu_{0.59}Zn_{0.38}Fe_{0.02}Pb_{0.01}$
9	″	″	″	″	56.49	38.88	″	3.04	1.59	N. f.	$Cu_{0.58}Zn_{0.39}Fe_{0.02}Pb_{0.01}$
10	″	″	″	″	2.04	N. f.	95.74	N. f.	2.17	″	$Sn_{0.92}Cu_{0.04}Fe_{0.04}$

The tephra lithogenic gases were found to contain N_2, CO, CO_2, and $C_{1–4}$ hydrocarbons. The Erebus tephra gases have a composition and proportions between components to correlate them with products of crust–mantle interactions, rather closer to mantle formations proper. The carbon isotope composition in the tephra lies within the values determined for the so-called atomically dispersed form of carbon in present-day volcanic ejecta at the Pacific Ring of Fire, as well as for organoids of volcanic atmospheric electrogenic origin. Overall, the tephra studied here can be treated as an explosive, almost wholly glassy analogue of the anorthoclase lava phonolites that terminate the continuous sequence of magmatic differentiates known as the Erebus lineage.

ACKNOWLEDGMENTS

We extend our gratitude for cooperation and valuable recommendations to Dr. Ph.R. Kyle, New Mexico Institute of Mining and Technology, Socorro, U.S.; Prof. R.G. Iblaminov, Perm State University; Cand. Sci. (Geol.–Mineral.) D.V. Kiseleva, Institute of Geology and Geochemistry, Ural Branch RAS, Cand. Sci. (Geol.–Mineral.) A.A. Soboleva and Leading Chemical Engineer I.V. Smoleva, Institute of Geology, Komi Science Center, Ural Branch RAS.

REFERENCES

Boynton, W.V., Geochemistry of the rare earth elements: Meteorite studies, in *Rare Earth Element Geochemistry,* Amsterdam: Elsevier,1984, pp. 63–114.

Encyclopedia of Volcanoes, Sigurdsson, H., Houghton, B., Rymer, H., et al., Eds., Academic Press, 1999, pp. 1172–1177.

Esser, R.P., Kyle, Ph.R., and McIntosh, W.C., $^{40}Sr/^{39}Sr$ dating of the eruptive history of Mount Erebus, Antarctica: Volcano evolution, *Bull. Volcanol.,* 2004, vol. 66, pp. 671–686.

Haggerty, St. E., A diamond trilogy: Superplumes, supercontinents and supernovae, *Sciences,* 1999, vol. 285, pp. 851–860.

Harpel, C.J., Kyle, Ph.R., Esser, R.P., et al., $^{40}Ar/^{39}Ar$ dating of the eruptive history of the Mount Erebus, Antarctica: summit flows, tephra, and caldera collapse, *Bull. Volcanol.,* 2004, vol. 66, pp. 687–702.

Iacovino, K., Moore, G., Roggensack, K., et al., H_2O–CO_2 solubility in mafic alkaline magma: Applications to volatile sources and degassing behavior at Erebus volcano, Antarctica, *Contrib. Mineral. Petrol.,* 2013, vol. 166, pp. 845–860.

Iverson, N.A., Kyle, Ph.R., Dungar, N.W., and McIntosh, W.C., Eruptive history and magmatic stability of Erebus volcano, Antarctica: Insights from englacial tephra, *Geochemistry, Geophysics, Geosystems,* 2014, no. 15, pp. 1–23.

Karpov, G.A., Silaev, V.I., Anikin, L.P., et al., Explosive mineralization, in *Tolbachinskoe treshchinnoe izverzhenie 2012–2013 gg.* (Tolbachik Fissure Eruption of 2012–2013), Novosibirsk: SO RAN, 2017, pp. 241–255.

Kelly, P.J., Dunbar, N.W., Kyle, Ph.R., and McIntoch, W.C., Refinement of the late Quaternary geologic history of Erebus volcano using $^{40}Sr/^{39}Sr$ and ^{36}Cl determinations, *J. Volcanol. and Geotherm. Res.,* 2008, vol. 177, pp. 569–577.

Kelly, P.J., Kyle, Ph.R., Dunbar, N.W., and Sims, K.W.W., Geochemistry and mineralogy of the phonolite lava lake, Erebus volcano, Antarctica: 1972–2004 and comparison with older lavas, *J. Volcanol. and Geotherm. Res.,* For submission to Special Issue on Erebus Volcano, 2007, pp. 1–56.

Kyle, Ph.R. and Jazek, A., Composition of three tephra layers from the Byrd Station ice core, Antarctica, *J. Volcanol. and Geotherm. Res.,* 1978, vol. 4, pp. 225–232.

Kyle, Ph.R., Moore, J.A., and Thirlwall, M.F., Petrologic evolution of anorthoclase phonolite lavas at Mount Erebus, Ross Island, Antarctica, *J. Petrol.,* 1992, vol. 33, no. 4, pp. 849–875.

Panter, K.S., Blusztayn, J., Hart, S.R., et al., The origin of HIMU in the SW Pacific: Evidence from intraplate volcanism in southern New Zealand and subantarctic islands, *J. Petrol.,* 2006, vol. 47, pp. 1673–1704.

Petrovsky, V.A., Silaev, V.I., Sukharev, A.E., et al., Fluid phases in carbonado and their genetic information content, *Geokhimiya,* 2008, no. 7, pp. 748–765.

Petrograficheskii kodeks Rossii. Magmaticheskie, metamorficheskie, metasomaticheskie, impaktnye obrazovaniya (Petrographic Code of Russia. Magmatic, Metamorphic, Metasomatic, and Impact Formations), 3rd Ed., rev. and suppl., St. Petersburg: VSEGEI, 2009.

Shcherbakov, Yu.G., A geochemical classification of elements, *Dokl. Akad. Nauk SSSR,* 1965, vol. 164, no. 4, pp. 917–920.

Shcherbakov, Yu.G., *Geochemical evolution and ore formations, in Problemy endogennogo rudoobrazovaniya i metallogenii* (Problems of Endogenous Mineralization and Metallogeny), Novosibirsk: Nauka, 1976, pp. 217–229.

Shcherbakov, Yu.G., The periodic system and the geochemical distribution of elements in space, *Geol. Geofiz.,* 1982. no. 1, pp. 77–87.

Silaev, V.I., Anikin, L.P., Vergasova, L.P., et al., Abiogenic organic polymers in ejecta of modern volcanism, *Vestnik Permskogo Universiteta, Geologiya,* 2016, no. 3, pp. 21–33.

Silaev, V.I., Anikin, L.P., Shanina, S.N., et al., *Abiogennye kondensirovannye organicheskie polimery v produktakh sovremennogo vulkanizma v svyazi s problemoi vozniknoveniya zhizni na Zemle* (Abiogenic Condensed Organic Polymers in Ejecta of Recent Volcanism in Relation to the Origin of Life on Earth), Syktyvkar: Geoprint, 2018.

Silaev, V.I., Karpov, G.A., Anikin, L.P., Vasiliev, E.A., Vergasova, L.P., and Smoleva, I.V., Mineral phase paragenesis in explosive ejecta discharged by recent eruptions in Kamchatka and the Kuril Islands. Part 1. Diamonds, carbonaceous phases, and condensed organoids, *J. Volcanol. Seismol.,* 2019, vol. 13, no. 5, pp. 323–334.

Stothers, R.B. and Rampino, M.R., Volcanic eruptions in the Mediterranean before A.D.630, *J. Geophys. Res.,* 1983, vol. 88, pp. 6357–6370.

Tazieff, H., *Erebus: Volcan antarctique,* Arthaud, 1978.

Wood, D.A., The application of a Th-Hf-Ta diagram to problems of tectonomagmatic classification and to establishing the nature of crustal contamination of basaltic lavas of the British Tertiary Volcanic Province, *Earth Planet. Sci. Lett.,* 1980, vol. 50, pp. 11–30.

Translated by A. Petrosyan